HHS Public Access

Author manuscript

Gene Ther. Author manuscript; available in PMC 2015 September 01.

Published in final edited form as:

Gene Ther. 2015 March ; 22(3): 247–256. doi:10.1038/gt.2014.110.

The systemic delivery of an oncolytic adenovirus expressing decorin inhibits bone metastasis in a mouse model of human prostate cancer

Weidong Xu, PhD[1], **Thomas Neill, PhD**[2], **Yuefeng Yang, PhD**[1], **Zebin Hu, PhD**[3], **Elyse Cleveland, BS**[4], **Ying Wu, PhD**[5], **Ryan Hutten, BS**[5], **Xianghui Xiao, PhD**[6], **Stuart R. Stock, PhD**[7], **Daniel Shevrin, MD**[8], **Karen Kaul, MD PhD**[4], **Charles Brendler, MD**[9], **Renato V. Iozzo, MD**[2], and **Prem Seth, PhD**[1,*]

[1]Gene Therapy Program, Department of Medicine, North Shore Research Institute, Evanston, IL, an affiliate of the University of Chicago, IL

[2]Department of Pathology, Anatomy, and Cell Biology and the Cancer Cell Biology and Signaling Program, Kimmel Cancer Center, Thomas Jefferson University, Philadelphia, PA

[3]1st Division of in Vitro Diagnostic Reagents, National Institutes for Food and Drug Control, Beijing, China

[4]Department of Pathology, North Shore Research Institute, Evanston, IL

[5]Image processing Lab, Department of Radiology, North Shore Research Institute, Evanston, IL

[6]Advanced Photon Source, Argonne National Lab., Lemont, IL

[7]Department of Cell and Molecular Biology, Northwestern University, Chicago, IL

[8]Department of Medicine, North Shore University Health Sytem, Evanston, IL

[9]Department of Surgery, North Shore University Health Sytem, Evanston, IL

Abstract

In an effort to develop a new therapy for prostate cancer bone metastases, we have created Ad.dcn, a recombinant oncolytic adenovirus carrying the human decorin gene. Infection of PC-3 and DU-145, the human prostate tumor cells, with Ad.dcn or a non-replicating adenovirus Ad(E1-).dcn resulted in decorin expression; Ad.dcn produced high viral titers and cytotoxicity in human prostate tumor cells. Adenoviral-mediated decorin expression inhibited Met, the Wnt/β-catenin signaling axis, vascular endothelial growth factor A, reduced mitochondrial DNA levels, and inhibited tumor cell migration. To examine the anti-tumor response of Ad.dcn, PC-3-luc cells were inoculated in the left heart ventricle to establish bone metastases in nude mice. Ad.dcn, in

[*]**Corresponding Author:** Prem Seth, PhD, Gene Therapy Program, Department of Medicine, North Shore Research Institute, an affiliate of the University of Chicago, Evanston Hospital, 2650 Ridge Ave, Room B 652, Evanston, IL 60201. Phone (847) 570-2378. pseth@northshore.org.

CONFLICT OF INTEREST

None of the authors have any conflict of interest.

conjunction with control replicating and non-replicating vectors were injected via tail vein. The real-time monitoring of mice, once a week, by bioluminescence imaging and X-ray radiography showed that Ad.dcn produced significant inhibition of skeletal metastases. Analyses of the mice at the terminal time point indicated a significant reduction in the tumor burden, osteoclast number, serum TRACP 5b levels, osteocalcin levels, hypercalcemia, inhibition of cancer cachexia, and an increase in the animal survival. Based on these studies, we believe that Ad.dcn can be developed as a potential new therapy for prostate cancer bone metastasis.

Keywords

Oncolytic adenovirus; prostate cancer bone metastases; decorin

INTRODUCTION

Prostate cancer (PCa) is the second leading cause of cancer-related deaths in men in the United States.[1] Following initial standard treatments and subsequent androgen deprivation therapy, many patients develop castration resistant prostate cancer (CRPC). During its advanced stage, PCa often metastasizes to bone, producing bone pain and spinal cord compression, and resulting in high morbidity and mortality.[2] Existing therapies for the advanced PCa and bone metastases are only palliative in nature.[3–8] Two currently available bone protecting modalities, denosumab, an antibody against the receptor activator of nuclear factor kappa-B ligand (RANKL), and bisphosphonates are quite effective in inhibiting bone resorption and controlling skeletal-related events. However, they have minimal impact on the patient's survival.[4, 9, 10] Therefore, the development of novel, highly effective and potentially curative treatment of PCa bone metastases is a major unmet healthcare need.

Recently, there has been an interest in developing oncolytic adenoviral vectors for the treatment of cancer, and their application in targeting the bone metastases is only beginning to be explored.[11–16] To target skeletal metastases, our laboratory is interested in developing recombinant oncolytic adenoviruses that will kill the cancer cells and simultaneously produce therapeutic proteins that target the tumor-bone environment.[16, 17] Towards that end, we have now created Ad.dcn, an oncolytic adenovirus carrying the decorin (*DCN*) gene. Decorin is a small leucine-rich proteoglycan, and low levels of decorin are generally considered a poor prognostic marker of prostate cancer.[18, 19] Decorin is an attractive candidate as decorin protein can target and suppress multiple tyrosine kinase receptors including Met, the Wnt/β-catenin signaling pathway, and effectively inhibits the angiogenic network[18, 20–23], all of which are known to promote prostate cancer tumorigenesis and bone metastases.[24–27] Interestingly, decorin can also target the tumor-bone microenvironment and inhibit osteoclastogenesis, and promote the osteoblastogenesis. [28, 29] The systemic delivery of decorin protein, or local delivery of adenoviral vectors expressing decorin, can inhibit tumor growth.[30–32] However, the systemic application of oncolytic adenoviruses expressing decorin for targeting bone metastases has not been previously investigated. In this report, we describe the construction of Ad.dcn and *in vitro* studies evaluating its replication potential and its ability to produce functional decorin in prostate tumor cells. We further describe the effect of systemic administration of Ad.dcn to inhibit PCa bone metastases and tumor-

induced bone destructions in a mouse model. Based on our results described here, we believe that Ad.dcn can be potentially developed as an anti-tumor agent for robust targeting of PCa bone metastases.

RESULTS

Construction of Ad.dcn, Ad.dcn replication, viral-induced cytotoxicity and decorin production in the prostate tumor cell lines

Ad.dcn, a recombinant oncolytic adenovirus containing the decorin gene, and Ad(E1-).dcn, a non-replicating adenovirus containing the decorin gene, were created as described in the Materials and Methods. The schematic diagrams of Ad.dcn, Ad(E1-).dcn, Ad.luc (an oncolytic adenovirus carrying luciferase 2 gene) and Ad(E1-).luc (a non-replicating adenovirus carrying luciferase 2 gene) are shown in Figure 1a. The replication potential and the viral induced cytotoxicity of the Ad.dcn and Ad(E1-).dcn, along with Ad.luc, Ad(E1-).luc, and Ad(E1-).null were determined in two human prostate tumor cell lines, PC-3 and DU-145, and in a mouse prostate tumor cell line TRAMP-C2. Viral titers of Ad.dcn and Ad.luc were about 2000-times higher than those of replication-deficient Ad(E1-).null, Ad(E1-).dcn and Ad(E1-).luc in PC-3 cells and DU-145 cells (Figure 1b). Ad.dcn and Ad.luc produced a similar dose-dependent cytotoxicity in PC-3 cells (Figure 1c) and in DU-145 cells (Figure 1d). In TRAMP-C2 cells, minimum viral replication (Figure 1b), and cell cytotoxicity (data not shown) were produced by adenoviruses.

Infection of the prostate tumor cell lines with Ad.dcn or Ad(E1-).dcn produced decorin protein, which was detected in both the cell lysates, and in the extracellular media (Figure 1e). The amounts of decorin protein released in the media from Ad.dcn and Ad(E1-).dcn-infected cells were similar (in the range of 1–4 μg/ml) (Figure 1f). These results suggest that Ad.dcn can replicate and produce cytotoxicity in human prostate tumor cells, and that both Ad.dcn and Ad(E1-).dcn produce decorin protein in prostate tumor cells.

Adenoviral-expressed decorin reduces Met, β-catenin and vascular endothelial growth factorA (VEGFA) expression, and migration of human prostate tumor cells

To examine if the decorin protein produced by the recombinant adenoviral vectors is functionally active, PC-3 cells were infected with Ad(E1-).dcn, and analyzed for multiple known target genes, *MET*, *CTNNB1 (catenin (cadherin-associated protein) beta 1*), and *VEGFA*, by qPCR. The results indicated that Ad(E1-).dcn infection resulted in a significant down-regulation of *MET* ($p<0.01$), *CTNNB1* ($p<0.001$) and *VEGFA* ($p<0.01$) at the mRNA level (Figure 2a) following authentication of robust *DCN* mRNA expression. The Ad(E1-).dcn-infection also resulted in significant reductions of Met, β-catenin, and VEGFA protein expression ($p<0.001$) (Figure 2 b–c). Ad(E1-).dcn-infection of PC-3 cells also reduced mtDNA levels ($p<0.01$) (Figure 2d), indicating induction of decorin-induced mitochondrial autophagy. Moreover, decorin containing conditioned media (about 3 μg/ml) inhibited cell migration in a transwell migration assay ($p<0.01$) (Figure 2e). In a wound-healing assay, the decorin containing media also showed significant reductions in the wound areas filled at 16 hours ($p<0.01$), and at 24 hours ($p<0.001$) (Figure 2f). These results indicate that adenoviral-mediated decorin production is functionally and biologically active.

Systemic administration of Ad.dcn inhibits the progression of established prostate cancer bone metastases

Next, the anti-tumor effects of Ad.dcn in a prostate cancer bone metastasis model were examined. PC-3-luc cells were inoculated into the left heart ventricle of male nude mice. The mice were subjected to bioluminescence imaging (BLI) on day 9 and divided into five treatment groups. Mice were intravenously administered with either buffer, Ad.dcn, Ad(E1-).dcn, Ad.luc or Ad(E1-).luc on day 10, day 13, and day 16 (2.5×10^{10} Viral particles (VPs)/mouse each dose; a total of 7.5×10^{10} VPs/mouse). BLI signals were monitored once a week. Whole-body dorsal and ventral BLI images of representative mice from the buffer, Ad.dcn and Ad(E1-).dcn treatment groups on day 9, day 30 and day 51; and on day 51 for Ad.luc2 and Ad(E1-).luc2 treatment groups are shown in Figure 3a (dorsal view) and Figure 3b (ventral view). Due to the hepatic uptake of the adenoviruses following intravenous injections during the earlier time points[17, 33], the BLI of Ad.luc and Ad(E1-).luc treated groups produced strong luciferase expression in the liver, thus masking the BLI signal in the skeletal tumors. However, on day 51, the BLI signal in the hind limbs was quite distinct from the liver signal in the Ad.luc and Ad(E1-).luc-treated mice (Figure 3a and 3b). The resultant signal intensities of dorsal and ventral hind limbs within regions of interest (ROIs) were quantified. Ad.dcn and Ad(E1-).dcn groups exhibited significant reductions in the BLI signal over the course of the study ($p<0.001$) (Figure 3c). Quantification of the fold-increases of BLI signal from day 9 to day 51 indicated that Ad.dcn treatment group produced significant reduction in the skeletal tumor growth ($p<0.01$), and that Ad(E1-).dcn and Ad.luc were also effective ($p<0.05$) (Figure 3d). No significant inhibition of fold-increases was observed by the Ad(E1-).luc treatment.

Bone metastases were further examined using radiographic measurements taken weekly from day 21 onwards. The representative X-ray images on day 21, day 42 and day 60 from each group are shown in Figure 4a. Osteolytic lesions on the skeletal tumors are marked by yellow arrows. The skeletal tumor sizes were measured in both hind limbs of each mouse, over the course of the study. As shown in Figure 4b, Ad.dcn, Ad(E1-).dcn, and Ad.luc treatments resulted in the inhibition of tumor progression. However, the Ad.dcn group was the most effective ($p<0.001$ vs. buffer), and produced better responses than Ad.luc ($p<0.01$ Ad.luc vs buffer; $p<0.05$ Ad.dcn vs Ad.luc) or Ad(E1-).dcn ($p<0.05$ Ad(E1-).dcn vs buffer; $p<0.01$ Ad.dcn vs. Ad(E1-).dcn). Moreover, on day 60, only the Ad.dcn treatment resulted in significant inhibition of tumor size ($p<0.05$) (Figure 4c), and produced a significant number of skeletal tumor-free mice ($p<0.05$) (Figure 4d). There was no significant inhibition of tumor growth by Ad(E1-).luc treatment. These results suggest that Ad.dcn, Ad.luc and Ad(E1-).dcn treatments all resulted in the inhibition of bone metastases as examined by the BLI and X-ray radiography, and among the three vectors, Ad.dcn is the most effective in inhibiting skeletal metastases.

Systemic administration of Ad.dcn reduces tumor burden, inhibits bone destruction, and increases animal survival

The tumor burden at the terminal time point (day 62) was examined by histomorphometric analyses. The representative H&E staining of tibia and femur median sagittal sections from each group are shown in Figure 5a. The tumor areas were outlined with a yellow line (Figure

5a) and quantified. The buffer group had a large tumor burden, and the treatment of mice with Ad.dcn resulted in a significant reduction in tumor burden ($p<0.05$) (Figure 5b) and produced a significant tumor-free incidence ($p<0.05$) (Figure 5c). Analysis of serum decorin protein levels (on day 62) indicated that both the Ad.dcn and Ad(E1-).dcn treated groups contained decorin, while no decorin protein was detected in the other treatment groups (Figure 5d).

The osteolytic bone destruction in the distal femur was further examined by synchrotron micro computed tomography (microCT). The reconstructed slices near the growth plate region and 1.45 mm below the growth plate showed extensive trabecular and cortical bone destruction in the buffer and Ad(E1-).luc treated groups (Figure 5e, top two panels). The 3D renderings of the bone volume also showed lesions in the buffer and Ad(E1-).luc groups (Figure 5e, bottom panel). However, normal slices and bone architecture were observed in the bones examined from Ad.dcn, Ad(E1-).dcn and Ad.luc treated groups (Figure 5e).

To further evaluate the effects of adenoviral vectors on bone resorption/formation, several relevant biomarkers were examined. These included tartarate resistant acid phosphatase (TRAP) positive osteoclasts in the bone/tumor interface and serum TRACP 5b levels as indicators of osteolytic bone destruction, serum osteocalcin as a marker of bone turn over, and serum calcium levels as an indicator of bone destruction. Representative bone samples stained for TRAP positive osteoclasts along the bone/tumor interface are shown in Figure 6a, with arrows pointing to the multinucleated mature osteoclasts. Among all the treatment groups, only Ad.dcn treatment resulted in a significant reduction in the osteoclast number, compared to the buffer group ($p<0.05$) (Figure 6b). Treatment with Ad.dcn, Ad.luc, or Ad(E1-).dcn resulted in significant reductions in the TRACP 5b levels (Ad.dcn vs buffer $p<0.001$; Ad(E1-).dcn vs buffer $p<0.01$; Ad.luc vs buffer $p<0.01$) (Figure 6c). Ad.dcn, Ad(E1-).dcn and Ad.luc treatments also resulted in the reduction of serum osteocalcin levels; Ad.dcn and Ad.luc treatments were relatively more effective ($p<0.001$) than Ad(E1-).dcn ($p<0.01$) (Figure 6d). Ad.dcn treatment was effective in inhibiting hypercalcemia ($p<0.001$), although both Ad.luc ($p<0.01$) and Ad(E1-).dcn ($p<0.05$) treatments were also highly-effective in reducing calcium levels (Figure 6e). Ad(E1-).luc treatment had no significant effect in the assays conducted above (osteoclast number, TRACP 5b, osteocalcin and calcium levels) (Figure 6 b–e).

Animal body weight was monitored weekly, as an indicator of cancer cachexia. In the buffer group, the mice began to lose body weight from day 51 onwards. By day 62, there was a significant reduction in the body weight of mice in the buffer group compared to the normal mice ($p<0.01$) and the Ad.dcn treatment group ($p<0.05$) (Figure 6f); only the Ad.dcn treatment group produced a significant survival advantage over the buffer group (as measured by the loss of 10% body weight) ($p<0.05$) (data not shown).

DISCUSSION

The major finding of our study is that the systemic delivery of Ad.dcn, an oncolytic adenovirus expressing decorin, is effective in inhibiting skeletal metastases and the bone destruction in a mouse model of human prostate cancer. In multiple assays, the Ad.dcn was

more potent than both Ad(E1-).dcn, a non replicating adenovirus expressing decorin, and Ad.luc, a control oncolytic adenovirus (Table 1). Thus, adenoviral replication, coupled with concomitant decorin production in Ad.dcn, is critical in producing strong anti-tumor responses and a significant number of tumor-free mice, and inhibiting bone destruction, resulting in an increase in the animal survival.

Based on our findings, we propose the following model of Ad.dcn-mediated inhibition of bone metastases. Upon intravenous delivery of Ad.dcn in skeletal tumor bearing mice, the virus is taken up by the skeletal tumors producing viral replication and tumor-destruction. Ad.dcn infected tumor cells produce decorin that is released into the tumor microenvironment, and targets multiple tumor and stromal components, and interrupts the vicious cycle between tumor cells and the surrounding stromal cells, resulting in the inhibition of tumor growth and tumor-induced bone destruction. In support of this model, we have shown that the infection of prostate tumor cells with Ad.dcn resulted in viral replication, tumor cell-killing, and decorin production, which is released into the extracellular compartment. The prostate tumor cells ectopically expressing decorin responded in an autocrine manner resulting in the down regulation of several tumor/bone metastases promoting decorin targets. These targets included, *MET*, that encodes for a tyrosine kinase receptor that is often activated in prostate cancer; *CTNNB1*, that encodes for β-catenin, the aberrant expression of β-catenin is associated with the prostate tumor growth and metastases; and *VEGFA*, the protein product of which is known to promote angiogenesis. [6, 18, 20–27, 34, 35] The Ad.dcn-mediated decorin released in tumor-microenvironment will also target the osteoclasts and the osteoblasts and inhibit osteoclast activity and promote the osteoblastogenesis.[28, 29] Ad.dcn-mediated decorin production was shown to inhibit the prostate tumor cell migration, a step that is necessary to establish the skeletal metastases.[36] Interestingly, decorin expression in prostate tumor cells also resulted in decreased mtDNA content, a marker for mitochondrial turnover and degradation[23, 37, 38], consistent with the earlier studies in which soluble decorin was shown to evoke mitochondrial autophagy (mitophagy) in breast carcinoma cells via a novel mitophagic effector, mitostatin.[39] Ad.dcn-induced authophagy of the prostate tumor cells *in vivo* could potentially stimulate the cell-mediated immune responses against the tumor cells and enhance the anti-tumor-responses.[40] The ability of Ad(E1-).dcn to inhibit bone metastases, albeit weaker than Ad.dcn, is consistent with the proposed model, and are in agreement with the previous studies in which decorin was shown to inhibit the tumor growth of colon and breast carcinoma.[30, 31]

While our *in vitro* experiments and the *in vivo* studies describing the anti-tumor responses of Ad.dcn corroborate with our proposed model we realize that some of the steps need to be investigated further *in vivo* in a bone metastasis model. It will be also interesting to examine if the vector-mediated decorin expression can also enhance the intratumoral adenoviral spread, and hence its oncolytic potential, as previously suggested.[32] Since, the human adenoviruses replicate poorly in mouse prostate tumor cells studied here, we need to identify an immune-competent syngeneic mouse bone metastases tumor model to examine the anti-tumor responses of Ad.dcn, and to examine additional immunotherapy strategies to further enhance the anti-tumor responses of Ad.dcn. Given that Ad.dcn, can directly kill cancer

cells, and can simultaneously target multiple tumor promoting signaling pathways, we believe that Ad.dcn can be potentially developed for the treatment of PCa skeletal metastases.

MATERIALS AND METHODS

Cell lines and adenoviruses

Human prostate tumor cell lines PC-3 and DU-145, and a mouse prostate tumor cell line TRAMP-C2 were obtained from ATCC (Manassas, VA). PC-3-luc cell line was kindly provided by Kenneth Pienta (University of Michigan, Ann Arbor, MI). All prostate tumor cell lines were maintained in RPMI-1640 media containing 10% fetal calf serum. To create Ad.dcn, the decorin gene was cloned in a shuttle vector and subjected to homologous recombination with adenoviral genomic DNA derived from adenoviral mutant *dl*01/07, using published methods.[41] To create Ad(E1-).dcn, an AdEasy system was used for homologous recombination.[42] Ad(E1-).null (the non-replicating adenovirus without any foreign trangene), Ad(E1-).luc (the non-replicating adenovirus containing firefly luciferase2 gene), and Ad.luc (the conditionally replicating adenovirus containing firefly luciferase2 gene) have been previously described.[33, 43, 44] All adenoviral vectors were amplified in HEK293 cells (ATCC), and purified as described earlier.[43]

Adenoviral replication and cytotoxicity assays

Tumor cells were exposed to viral vectors (2.5×10^4 VPs/cell) for 3 or 48 hours, and the viral burst sizes in HEK293 cells as a indicators of viral replication were measured using Adeno-X Rapid Titer Kit (Clontech, Mountain view, CA) as described previously.[16, 45] For cytotoxicity assays, cells were exposed to various concentrations of viral vectors for 7 days, and cell survival was examined using the sulforhodamine B staining method as described earlier.[16]

Adenoviral-mediated decorin expression

Cells were plated in 6-well dishes (5×10^5 cells/well). The following day, cells were infected with viral vectors (2.5×10^3 VPs/cell). After 24 hours, the media was changed to serum free media, and the incubations continued for another 24 hours. The media and the cell lysates were subjected to western blot analyses using published methods[16] except that the blots were probed with antibodies against human decorin (R&D systems, Minneapolis, MN). Decorin levels in the media were examined by ELISA using mouse anti-human decorin (R&D systems, Minneapolis, MN) and biotinylated mouse anti-human decorin (R&D systems, Minneapolis, MN), using a previously described method [16].

Gene expression analysis of canonical decorin target genes following infection with Ad(E1-).dcn

PC-3 cells were infected with either Ad(E1-).null or Ad(E1-).dcn (2.5×10^3 VPs/cell). To perform quantitative RT-PCR (qPCR) of *decorin* and decorin-regulated genes, *MET*, *CTNNB1*, and *VEGFA*, RNA were harvested and cDNA libraries generated after 48 hours post infection. All samples were subjected to a DNase I digestion to eliminate potentially contaminating genomic DNA and viral plasmids prior to cDNA synthesis and qPCR

analysis. *ACTB* served as the endogenous housekeeping gene. Fold changes were determined by the comparative ΔΔCt method.

Met, β-catenin and vascular VEGFA levels following infection with Ad(E1-).dcn

PC-3 cells were infected with 2.5×10^3 VPs/cell of Ad(E1-).null or Ad(E1-).dcn, and 48 hours later the lysates were harvested. Western blot analysis for Met, β-catenin, VEGFA and GAPDH were performed as previously described.[23, 46]

Mitochondrial DNA (mtDNA) analysis following infection with Ad(E1-).dcn

PC-3 cells were infected with Ad(E1-).null or Ad(E1-).dcn (2.5×10^3 VPs/cell) for 48 hours. Genomic DNA (gDNA) and mtDNA were isolated and interrogated via qPCR, as done previously[39], with mitochondrial encoded NADH dehydrogenase I (*ND1*) serving as a mtDNA marker, and lipoprotein lipase (*LPL*) for gDNA analysis and normalization. Reported fold changes were determined by the comparative ΔΔCt method.

Transwell migration and wound healing assays

PC-3 cells were infected with 2.5×10^4 VPs/cell of Ad.luc or Ad.dcn for 6 hours. Cells were washed and incubations continued in serum free media for 24 hours. The conditioned media was collected and subjected to ultracentrifugation to remove adenoviral particles. For transwell migration assay, 5.0×10^4 PC-3 cells were plated into each transwell with conditioned media in the top chamber. After 16 hours, cells that migrated to the lower surface of the filter were stained using manufacturer's protocol (Fisher Scientific). The cells per field of view were counted using 100× magnification (2.54 mm^2 field area). Scratched wound healing assays were carried out on nearly confluent PC-3 cells grown in 6-well plates as described.[47] Conditioned media from mock, Ad.luc or Ad.dcn-infected PC-3 cells were added, and at 0 hours, 16 hours and 24 hours, live cell images were taken with a Nikon DS-Fi1 camera. Gap distances between the two margins of the wounds were measured using Nikon image software and the percentages of wound area filled determined.

Animal studies

All animal experimental procedures were approved by the Institutional Animal Care and Use Committee (IACUC) at North Shore University Health System.

Bone metastasis model and BLI

PC-3-luc cells (2.0×10^5/mouse) were injected into the left heart ventricle of four week old male nude mice (Nu/Nu) (Charles River laboratories, Wilmington, MA). On day 9, mice were subjected to BLI in the dorsal and ventral positions using Xenogen IVIS Spectrum imaging equipment (Caliper life sciences, Hopkinton, MA). The signal intensity was quantified within regions of interest (ROI) in both left and right hind limbs as previously described.[16] Mice that had flux in the range of $2.0\times10^5 - 1.0\times10^6$ photons/second were divided into various groups, with statistically indistinguishable BLI signals amongst each group. BLI was conducted weekly for the duration of the study.

X-ray radiography imaging

Mice were subjected to X-ray radiography on day 21, and weekly thereafter until day 60, using Faxitron (Faxitron X-ray Corporation, Wheeling, IL) as previously described [16]. Bone lesions were quantified in the femur and tibia of both hind limbs using Image J software (NIH, Bethesda, MD) as described earlier.[16, 48]

Bone histology and histomorphometric analysis

On day 62, mice were euthanized, and hind limbs were harvested, processed and stained with hematoxylin and eosin (H&E) as previously described.[16] Tumor burden per tibia/femur was quantified on H&E-stained sections as previously described.[16, 48] Multinucleated TRAP positive osteoclasts at the bone-tumor interface were stained and counted as described earlier.[48]

Synchrotron microCT

Synchrotron microCT was performed using beamline 2-BM of the Advanced Photon Source (APS) at Argonne National Laboratory (Lemont, IL) using the microCT instrument as previously described.[49] X-ray photons of 22 keV were used, and the isotropic volume element (voxel) size in the reconstructions was 1.45 μm. 3-D images of bone sections spanning 3.48 mm near/below the growth plate regions were constructed using MATLAB R2011a (The MathWorks, Inc, Natick, Massachusetts).

Quantification of serum TRACP 5b, osteocalcin, and calcium levels

At the terminal time point, blood was collected via cardiac puncture. The sera were obtained by centrifuging blood at 10K rpm for 5 minutes. Serum concentrations of TRACP 5b were measured by the MouseTRAP kit (Immunodiagnosticsystems, Phoenix, AZ) as described.[16] Osteocalcin levels were measured by BTI Mouse Osteocalcin EIA Kit (Biomedical Technologies, Ward Hill, MA) as described.[50] Calcium concentrations were measured using the QuantiChrom calcium assay kit (BioAssay Systems, Hayward, CA) as described.[16]

Statistical analysis

Data were presented as mean ± SEM and statistically analyzed using GraphPad Prism software version 5 (GraphPad software, San Diego, CA). Longitudinal data were analyzed using a two-way repeated measure ANOVA followed by Bonferroni post-hoc tests for the data obtained over the time course. For multiple group analyses, one-way ANOVA followed by Bonferroni post-hoc tests adjusting for multiplicity were performed. Student's *t*-tests were performed to compare two sets of data. A Fisher exact test was used for the tumor incidence data in the X-ray and histomorphometric analyses. A Log-rank (Mantel-Cox) test was performed to compare the survival distributions. Differences were considered significant at $p<0.05$.

ACKNOWLEDGEMENTS

The work was funded in part by the National Institutes of Health grant # R01CA12738 (P.S.), grant # RO1CA39481 (R.V.I.), and philanthropic support through John and Carol Walter Center for Urological Health, North Shore University Health System. Use of the Advanced Photon Source was supported by the U. S. Department of Energy, Office of Science, Office of Basic Energy Sciences, under Contract No. DE-AC02-06CH11357. We are

thankful to Janardan Khandekar, Theodore Mazzone, Bruce Brockstein and Michael Caplan for their continuous support.

REFERENCES

1. Cancer Facts and Figures. 2013. http://www.cancer.org/Research/cancer-facts-figures-2013
2. Coleman RE. Metastatic bone disease: clinical features, pathophysiology and treatment strategies. Cancer Treat Rev. 2001; 27(3):165–176. [PubMed: 11417967]
3. Sturge J, Caley MP, Waxman J. Bone metastasis in prostate cancer: emerging therapeutic strategies. Nat Rev Clin Oncol. 2011; 8(6):357–368. [PubMed: 21556025]
4. Gartrell BA, Saad F. Managing bone metastases and reducing skeletal related events in prostate cancer. Nat Rev Clin Oncol. 2014; 11(6):335–345. [PubMed: 24821212]
5. Deng X, He G, Liu J, Luo F, Peng X, Tang S, et al. Recent advances in bone-targeted therapies of metastatic prostate cancer. Cancer Treat Rev. 2014; 40(6):730–738. [PubMed: 24767837]
6. Camacho DF, Pienta KJ. A multi-targeted approach to treating bone metastases. Cancer Metastasis Rev. 2014
7. Suzman DL, Boikos SA, Carducci MA. Bone-targeting agents in prostate cancer. Cancer Metastasis Rev. 2014
8. Lee RJ, Smith MR. Targeting MET and vascular endothelial growth factor receptor signaling in castration-resistant prostate cancer. Cancer J. 2013; 19(1):90–98. [PubMed: 23337762]
9. Lipton A, Balakumaran A. Denosumab for the treatment of cancer therapy-induced bone loss and prevention of skeletal-related events in patients with solid tumors. Expert Rev Clin Pharmacol. 2012; 5(4):359–371. [PubMed: 22943116]
10. Fizazi K, Carducci M, Smith M, Damiao R, Brown J, Karsh L, et al. Denosumab versus zoledronic acid for treatment of bone metastases in men with castration-resistant prostate cancer: a randomised, double-blind study. Lancet. 2011; 377(9768):813–822. [PubMed: 21353695]
11. Bischoff JR, Kirn DH, Williams A, Heise C, Horn S, Muna M, et al. An adenovirus mutant that replicates selectively in p53-deficient human tumor cells. Science. 1996; 274(5286):373–376. [PubMed: 8832876]
12. Seth, P., editor. Adenoviruses : Basic Biology to Gene Therapy. Austin, TX: R G Landes Company; 1999.
13. Yamamoto M, Curiel DT. Current issues and future directions of oncolytic adenoviruses. Mol Ther. 2010; 18(2):243–250. [PubMed: 19935777]
14. Choi IK, Yun CO. Recent developments in oncolytic adenovirus-based immunotherapeutic agents for use against metastatic cancers. Cancer Gene Ther. 2013; 20(2):70–76. [PubMed: 23306610]
15. Schenk E, Essand M, Bangma CH, Barber C, Behr JP, Briggs S, et al. Clinical adenoviral gene therapy for prostate cancer. Hum Gene Ther. 2010; 21(7):807–813. [PubMed: 20001452]
16. Hu Z, Gupta J, Zhang Z, Gerseny H, Berg A, Chen YJ, et al. Systemic delivery of oncolytic adenoviruses targeting transforming growth factor-beta inhibits established bone metastasis in a prostate cancer mouse model. Hum Gene Ther. 2012; 23(8):871–882. [PubMed: 22551458]
17. Xu W, Zhang Z, Yang Y, Hu Z, Wang CH, Morgan M, et al. Ad5/48 hexon oncolytic virus expressing sTGFbetaRIIFc produces reduced hepatic and systemic toxicities and inhibits prostate cancer bone metastases. Mol Ther. 2014; 22(8):1504–1517. [PubMed: 24791939]
18. Edwards IJ. Proteoglycans in prostate cancer. Nat Rev Urol. 2012; 9(4):196–206. [PubMed: 22349653]
19. Henke A, Grace OC, Ashley GR, Stewart GD, Riddick AC, Yeun H, et al. Stromal expression of decorin, Semaphorin6D, SPARC, Sprouty1 and Tsukushi in developing prostate and decreased levels of decorin in prostate cancer. PLoS One. 2012; 7(8):e42516. [PubMed: 22880013]
20. Neill T, Schaefer L, Iozzo RV. Decorin: a guardian from the matrix. Am J Pathol. 2012; 181(2): 380–387. [PubMed: 22735579]
21. Sofeu Feugaing DD, Gotte M, Viola M. More than matrix: the multifaceted role of decorin in cancer. Eur J Cell Biol. 2013; 92(1):1–11. [PubMed: 23058688]

22. Neill T, Painter H, Buraschi S, Owens RT, Lisanti MP, Schaefer L, et al. Decorin antagonizes the angiogenic network: concurrent inhibition of Met, hypoxia inducible factor 1alpha, vascular endothelial growth factor A, and induction of thrombospondin-1 and TIMP3. J Biol Chem. 2012; 287(8):5492–5506. [PubMed: 22194599]
23. Buraschi S, Pal N, Tyler-Rubinstein N, Owens RT, Neill T, Iozzo RV. Decorin antagonizes Met receptor activity and down-regulates {beta}-catenin and Myc levels. J Biol Chem. 2010; 285(53): 42075–42785. [PubMed: 20974860]
24. Kypta RM, Waxman J. Wnt/beta-catenin signalling in prostate cancer. Nat Rev Urol. 2012
25. Cook LM, Shay G, Aruajo A, Lynch CC. Integrating new discoveries into the "vicious cycle" paradigm of prostate to bone metastases. Cancer Metastasis Rev. 2014
26. Varkaris A, Corn PG, Gaur S, Dayyani F, Logothetis CJ, Gallick GE. The role of HGF/c-Met signaling in prostate cancer progression and c-Met inhibitors in clinical trials. Expert Opin Investig Drugs. 2011; 20(12):1677–1684.
27. Zeng Y, Opeskin K, Goad J, Williams ED. Tumor-induced activation of lymphatic endothelial cells via vascular endothelial growth factor receptor-2 is critical for prostate cancer lymphatic metastasis. Cancer Res. 2006; 66(19):9566–9575. [PubMed: 17018613]
28. Li X, Ling W, Khan S, Yaccoby S. Therapeutic effects of intrabone and systemic mesenchymal stem cell cytotherapy on myeloma bone disease and tumor growth. J Bone Miner Res. 2012; 27(8):1635–1648. [PubMed: 22460389]
29. Li X, Pennisi A, Yaccoby S. Role of decorin in the antimyeloma effects of osteoblasts. Blood. 2008; 112(1):159–168. [PubMed: 18436739]
30. Reed CC, Gauldie J, Iozzo RV. Suppression of tumorigenicity by adenovirus-mediated gene transfer of decorin. Oncogene. 2002; 21(23):3688–3695. [PubMed: 12032837]
31. Goldoni S, Seidler DG, Heath J, Fassan M, Baffa R, Thakur ML, et al. An antimetastatic role for decorin in breast cancer. Am J Pathol. 2008; 173(3):844–855. [PubMed: 18688028]
32. Choi IK, Lee YS, Yoo JY, Yoon AR, Kim H, Kim DS, et al. Effect of decorin on overcoming the extracellular matrix barrier for oncolytic virotherapy. Gene Ther. 2010; 17(2):190–201. [PubMed: 19907500]
33. Zhang Z, Krimmel J, Hu Z, Seth P. Systemic Delivery of a Novel Liver-Detargeted Oncolytic Adenovirus Causes Reduced Liver Toxicity but Maintains the Antitumor Response in a Breast Cancer Bone Metastasis Model. Hum Gene Ther. 2011; 22:1137–1142. [PubMed: 21480822]
34. Aftab DT, McDonald DM. MET and VEGF: synergistic targets in castration-resistant prostate cancer. Clin Transl Oncol. 2011; 13(10):703–709. [PubMed: 21975330]
35. Guise T. Examining the metastatic niche: targeting the microenvironment. Semin Oncol. 2010; 37(Suppl 2):S2–S14. [PubMed: 21111245]
36. Chaffer CL, Weinberg RA. A perspective on cancer cell metastasis. Science. 2011; 331(6024): 1559–1564. [PubMed: 21436443]
37. Munesue S, Yoshitomi Y, Kusano Y, Koyama Y, Nishiyama A, Nakanishi H, et al. A novel function of syndecan-2, suppression of matrix metalloproteinase-2 activation, which causes suppression of metastasis. J Biol Chem. 2007; 282(38):28164–28174. [PubMed: 17623663]
38. Dagda RK, Cherra SJ 3rd, Kulich SM, Tandon A, Park D, Chu CT. Loss of PINK1 function promotes mitophagy through effects on oxidative stress and mitochondrial fission. J Biol Chem. 2009; 284(20):13843–13855. [PubMed: 19279012]
39. Neill T, Torres A, Buraschi S, Owens RT, Hoek JB, Baffa R, et al. Decorin induces mitophagy in breast carcinoma cells via peroxisome proliferator-activated receptor gamma coactivator-1alpha (PGC-1alpha) and mitostatin. J Biol Chem. 2014; 289(8):4952–4968. [PubMed: 24403067]
40. Ma Y, Galluzzi L, Zitvogel L, Kroemer G. Autophagy and cellular immune responses. Immunity. 2013; 39(2):211–227. [PubMed: 23973220]
41. Seth P, Wang ZG, Pister A, Zafar MB, Kim S, Guise T, et al. Development of oncolytic adenovirus armed with a fusion of soluble transforming growth factor-beta receptor II and human immunoglobulin Fc for breast cancer therapy. Hum Gene Ther. 2006; 17(11):1152–1160. [PubMed: 17032151]

42. Hu Z, Robbins JS, Pister A, Zafar MB, Zhang ZW, Gupta J, et al. A modified hTERT promoter-directed oncolytic adenovirus replication with concurrent inhibition of TGFbeta signaling for breast cancer therapy. Cancer Gene Ther. 2010; 17(4):235–243. [PubMed: 19798122]

43. Katayose D, Gudas J, Nguyen H, Srivastava S, Cowan KH, Seth P. Cytotoxic effects of adenovirus-mediated wild-type p53 protein expression in normal and tumor mammary epithelial cells. Clin Cancer Res. 1995; 1(8):889–897. [PubMed: 9816059]

44. Hu Z, Zhang Z, Guise T, Seth P. Systemic Delivery of an Oncolytic Adenovirus Expressing Soluble Transforming Growth Factor-beta Receptor II-Fc Fusion Protein Can Inhibit Breast Cancer Bone Metastasis in a Mouse Model. Hum Gene Ther. 2010; 21(11):1623–1629. [PubMed: 20712434]

45. Zhang Z, Hu Z, Gupta J, Krimmel JD, Gerseny HM, Berg AF, et al. Intravenous administration of adenoviruses targeting transforming growth factor beta signaling inhibits established bone metastases in 4T1 mouse mammary tumor model in an immunocompetent syngeneic host. Cancer Gene Ther. 2012; 19(9):630–636. [PubMed: 22744210]

46. Goldoni S, Humphries A, Nystrom A, Sattar S, Owens RT, McQuillan DJ, et al. Decorin is a novel antagonistic ligand of the Met receptor. J Cell Biol. 2009; 185(4):743–754. [PubMed: 19433454]

47. Cory G. Scratch-wound assay. Methods Mol Biol. 2011; 769:25–30. [PubMed: 21748666]

48. Hu Z, Gerseny H, Zhang Z, Chen YJ, Berg A, Stock S, et al. Oncolytic Adenovirus Expressing Soluble TGFbeta Receptor II-Fc-mediated Inhibition of Established Bone Metastases: A Safe and Effective Systemic Therapeutic Approach for Breast Cancer. Mol Ther. 2011; 9:1609–1618. [PubMed: 21712815]

49. Wang YX, Carlo FD, Mancini DC, McNulty I, Tieman B, Bresnahan J, et al. A high-throughput X-ray microtomography system at the Advanced Photon Source. Review of Scientific Instruments. 2001; 72(4):2062–2068.

50. Schneider A, Kalikin LM, Mattos AC, Keller ET, Allen MJ, Pienta KJ, et al. Bone turnover mediates preferential localization of prostate cancer in the skeleton. Endocrinology. 2005; 146(4): 1727–1736. [PubMed: 15637291]

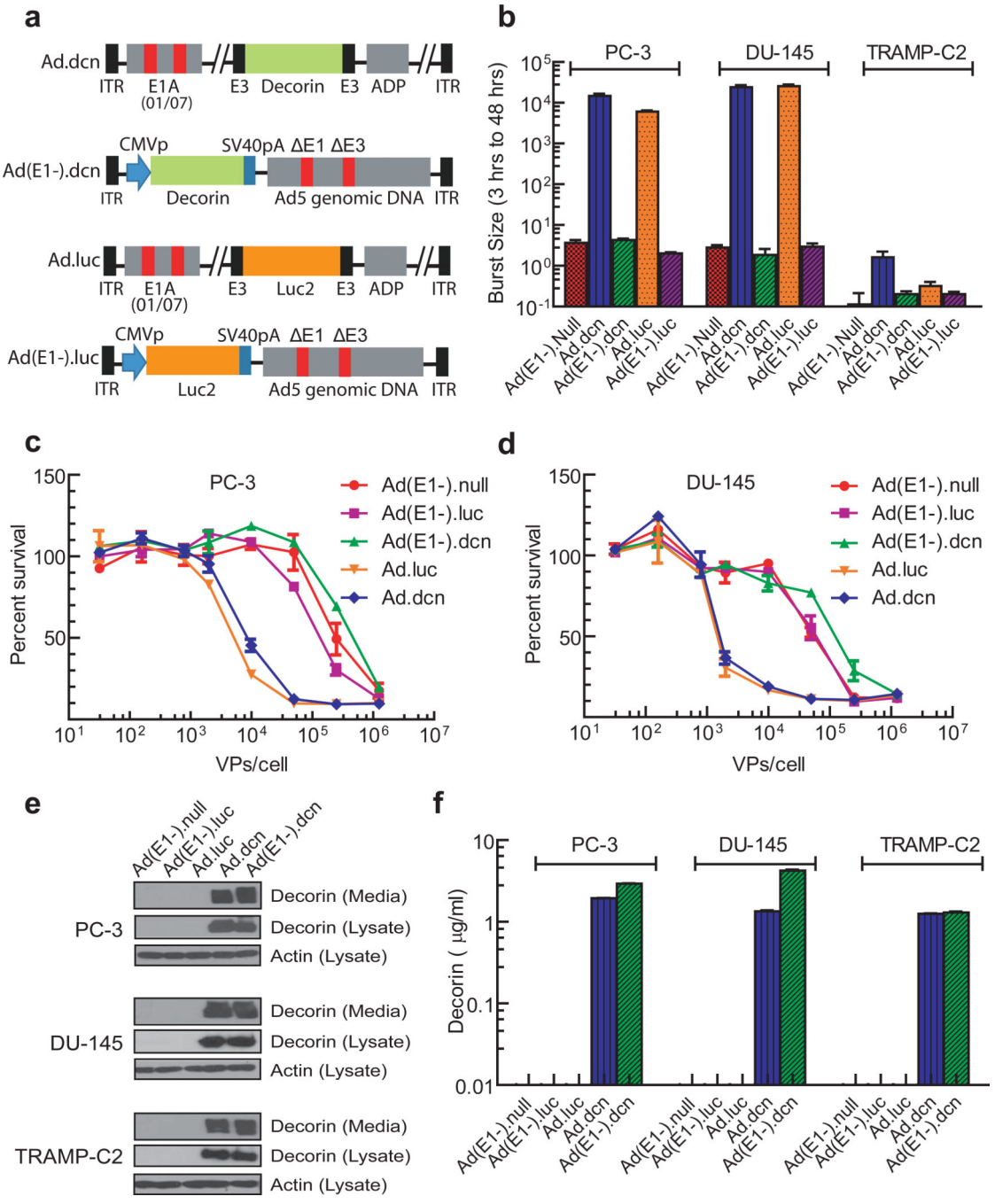

Figure 1.

Schematic diagrams of adenoviral vectors, viral replication, viral-induced cytotoxicity and protein expression in prostate tumor cell lines. (**a**) Schematic diagram of adenoviral constructs of Ad.dcn, Ad(E1-).dcn, Ad.luc and Ad(E1-).luc. Ad.dcn and Ad.luc have two small deletions, 01/07 (amino acids 4 to 25, and amino acids 111 to 123) in the E1A region, have deletion in E3 but contains ADP (adenoviral death protein). Ad(E1-).dcn, and Ad(E1-).luc are E1 and E3 minus. The maps are not drawn to scale. CMVp: CMV promoter, SV40pA: SV40 polyA, ITR: inverted terminal repeats. (**b**) Adenoviral replication in prostate

tumor cells. Tumor cells were infected with 2.5×10^4 VPs/cell for either 3 or 48 hours. The viral burst sizes were obtained in HEK293 cells, and the ratios of the burst sizes of 48 hours and 3 hour samples were calculated and are shown (**c, d**) Adenoviral-induced cytotoxicity in PC-3 and DU-145 cells. Cells were exposed to various doses of the viral vectors (in the range of 0.32×10^2 VPs/cell-1.25×10^6 VPs/cell) for 7 days, and the viral-induced cytotoxicity were measured by staining the cells with the sulforhodamine B (**e, f**) Adenoviral-mediated decorin expression in prostate tumor cells. Tumor cells were exposed to various adenoviral vectors (2.5×10^3 VPs/cell) for 48 hours (first 24 hours in the medium containing serum, and the second 24 hours in the media without serum). The cell lysates and the media were subjected to Western blot analyses for decorin **(e)**, the cell lysates were subjected Western blot analyses for actin **(e)**, and the media were subjected to ELISA for decorin expression **(f)** as described in Material and Methods.

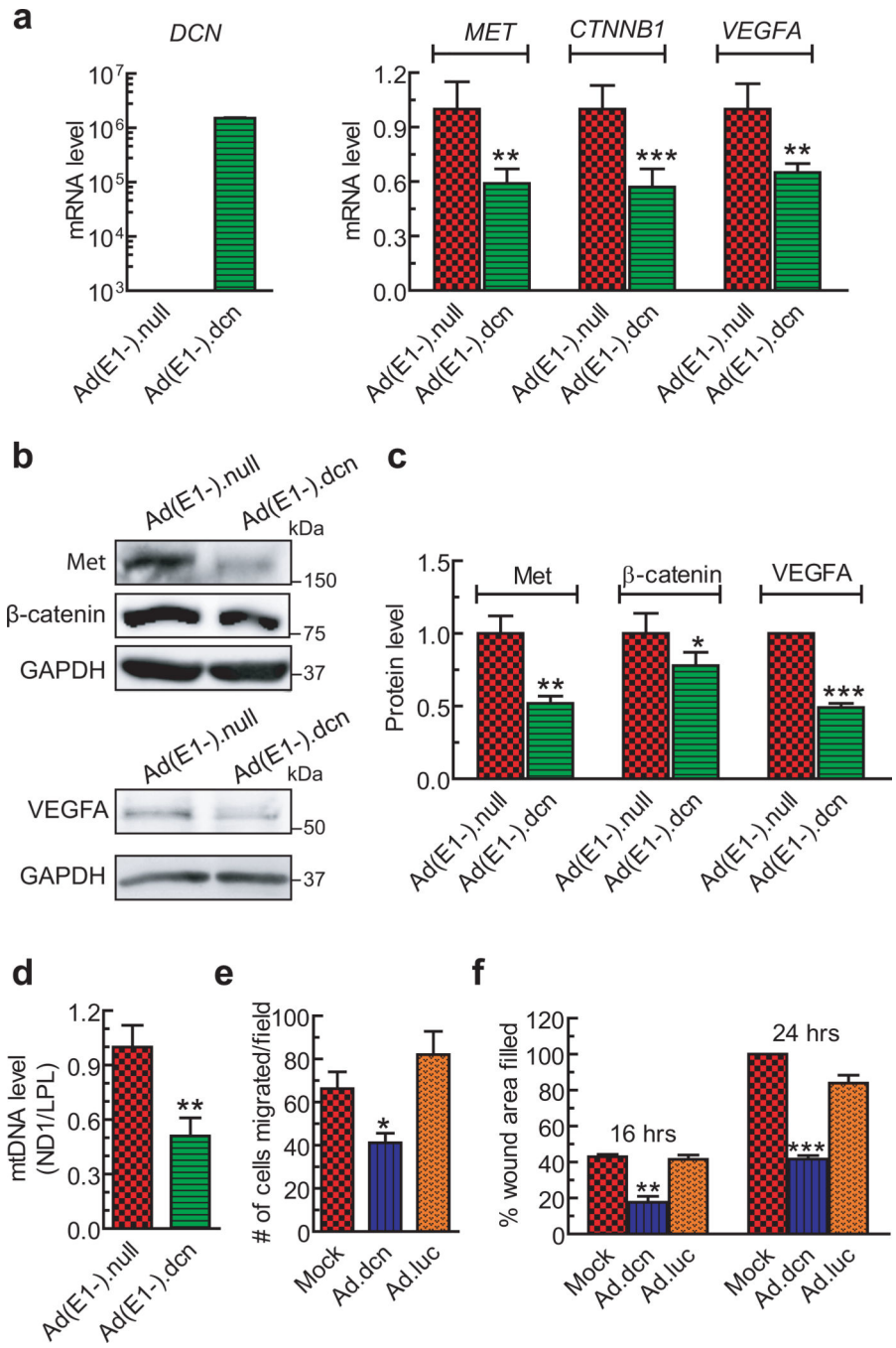

Figure 2.

Adenoviral-expressed decorin inhibits Met, β-catenin and VEGFA expression, and PC-3 cell migration. (**a**) Quantitative RT-PCR (qPCR) of known decorin-regulated genes (*MET*, *CTNNB1*, *VEGFA*) in PC-3 cells following a 48-hour infection with either Ad(E1-).null or Ad(E1-).dcn (2.5×10^3 VPs/cell). RNA isolates were subjected to DNAse I digestion prior to cDNA synthesis. (**b-c**) Ad(E1-).dcn significantly down-regulated Met, β-catenin, and VEGFA protein expression by an autocrine mechanism. Lysates were harvested following a 48-hour infection of PC-3 cells with either Ad(E1-).null or Ad(E1-).dcn using 2.5×10^3 VPs/

cell. GAPDH immunoreactivity served as the protein loading control. (**d**) PC-3 cells were infected with Ad(E1-).null or Ad(E1-).dcn (each used at 2.5×10^3 VPs/cell) for 48 hours and subjected to mtDNA analysis. Mitochondrial DNA was analyzed via qPCR by interrogating the mtDNA marker, *ND1*, in comparison with the genomic DNA marker, *LPL*, and fold changes were calculated by the comparative ΔΔCt method. (**e**) Quantification of PC-3 cells migrated in the transwell migration assay following treatment with conditioned media derived from mock, Ad.luc, or Ad.dcn infected PC-3 cells. The conditioned media obtained from PC3-cells infected with Ad.luc or Ad.dcn (2.5×10^4 VPs/cell) were incubated with PC-3 cells for 16 hours, and the cell migration was examined as described in Materials and Methods. (**f**) Quantification of the wound areas filled in wound healing assay following treatments with conditioned media obtained from mock, Ad.luc, or Ad.dcn infected PC-3 cells (2.5×10^4 VPs/cell). The conditioned media were exposed to the scratched PC-3 cells monolayer for 16 or 24 hours and the wound healing assays were performed as described in Materials and Methods. For **a-f**, three independent runs were performed and the results reported as fold changes±SEM (**a, c, d**) or mean±SEM (**e, f**). *P* value comparisons are shown for (**a**), (**c**), (**d**), (**e**), (**f**) (* represents $p<0.05$, ** represents $p<0.01$, *** represents $p<0.001$).

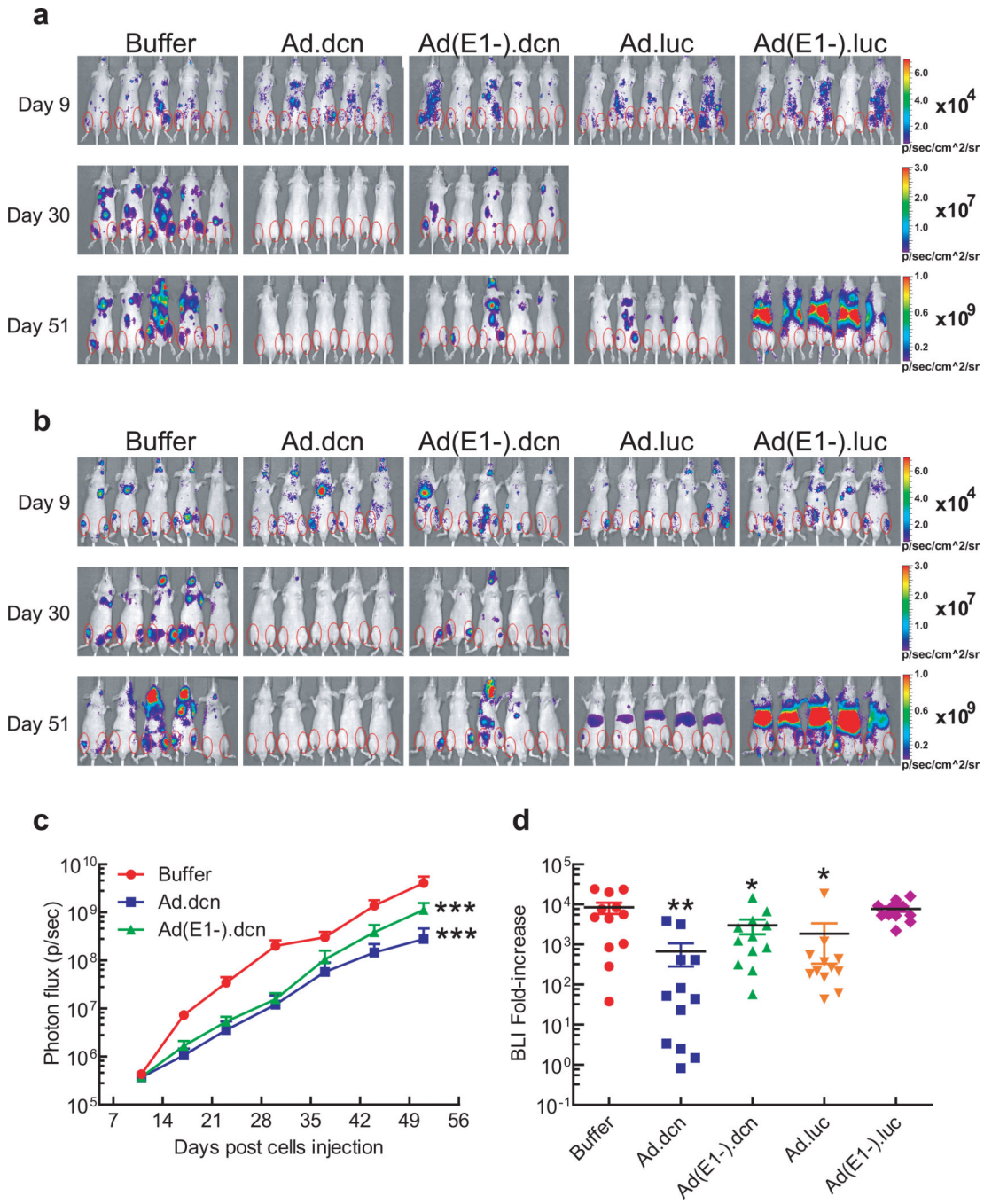

Figure 3.

Effect of adenoviral vectors on skeletal tumor progression by BLI analyses. (**a**) Representative whole body BLI images (dorsal view) on day 9, day 30 and day 51 are shown. (**b**) Representative whole body BLI images (ventral view) on day 9, day 30 and day 51 are shown. Regions of interest (ROIs) are shown with red circles in (**a**) and (**b**). (**c**) Skeletal tumor progression was monitored by the quantification of BLI signal intensities of combined dorsal and ventral hind limbs within ROIs and is shown. (**d**) Fold-increases of BLI signal intensity from day 9 to day 51 were calculated and are shown. *P* value

comparisons with buffer group are shown for C and D (* represents $p<0.05$, ** represents $p<0.01$, *** represents $p<0.001$). (n=12, each treatment group).

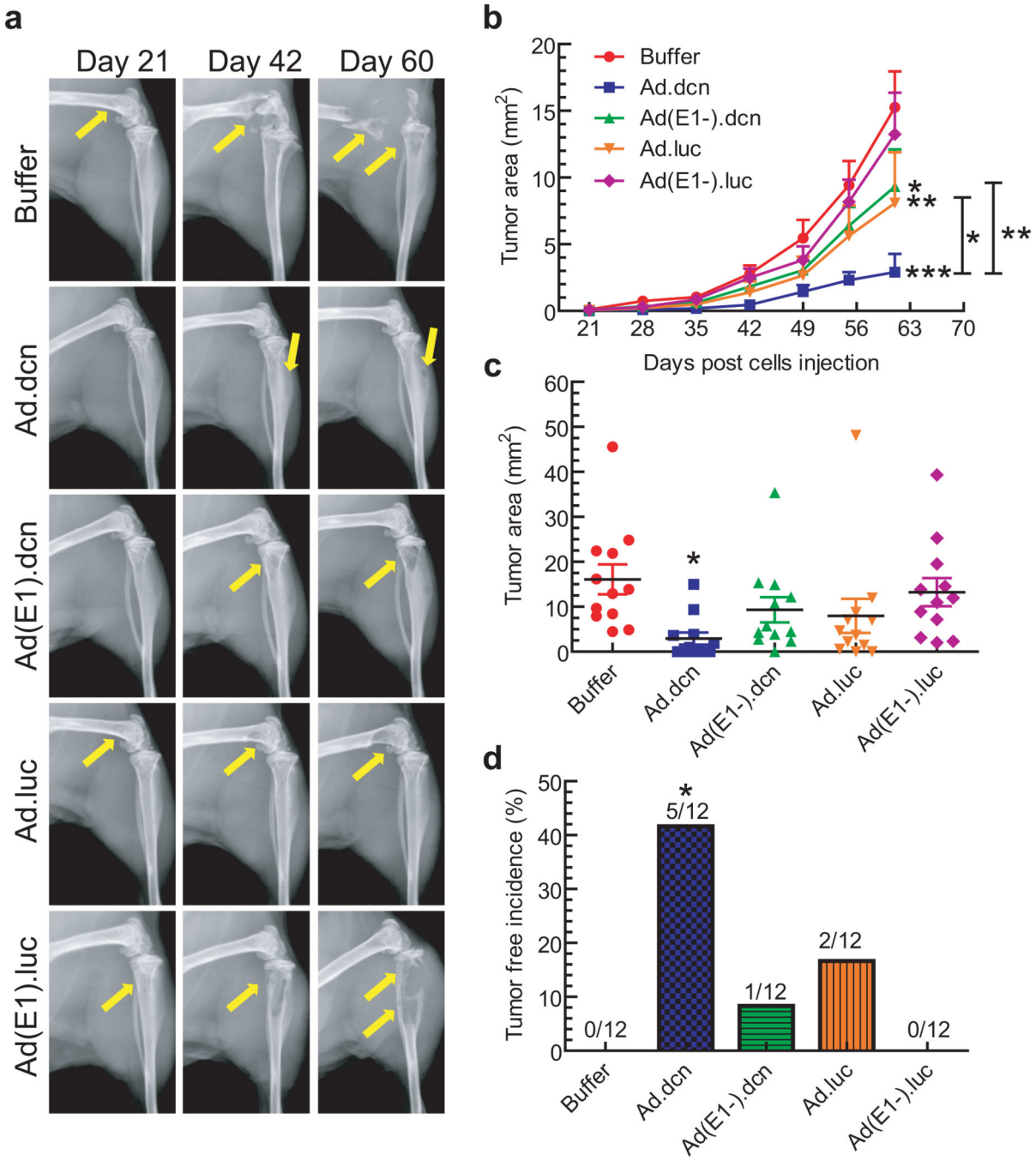

Figure 4.

Effect of adenoviral vectors on skeletal tumor progression by radiographic analyses. (**a**) Representative radiographs of mouse hind limbs on day 21, 42 and 60 are shown. Yellow arrows indicate the sites of osteolytic lesions. (**b**) Skeletal tumor progression was monitored by the quantification of radiography lesion sizes in both hind limb bones for the duration of the study and is shown. (**c**) Lesion sizes in the hind limb bones on day 60 were calculated and are shown. (**d**) Bone metastasis free incidences (mice without x-ray positive lesions) on day 60 are shown. *P* value comparisons with buffer group are shown for (**b**), (**c**) and (**d**), and

between Ad.dcn and Ad.luc, and between Ad.dcn and Ad(E1-).dcn for (**b**) (* represents $p<0.05$, ** represents $p<0.01$, *** represents $p<0.001$). (n=12, each of the treatment group).

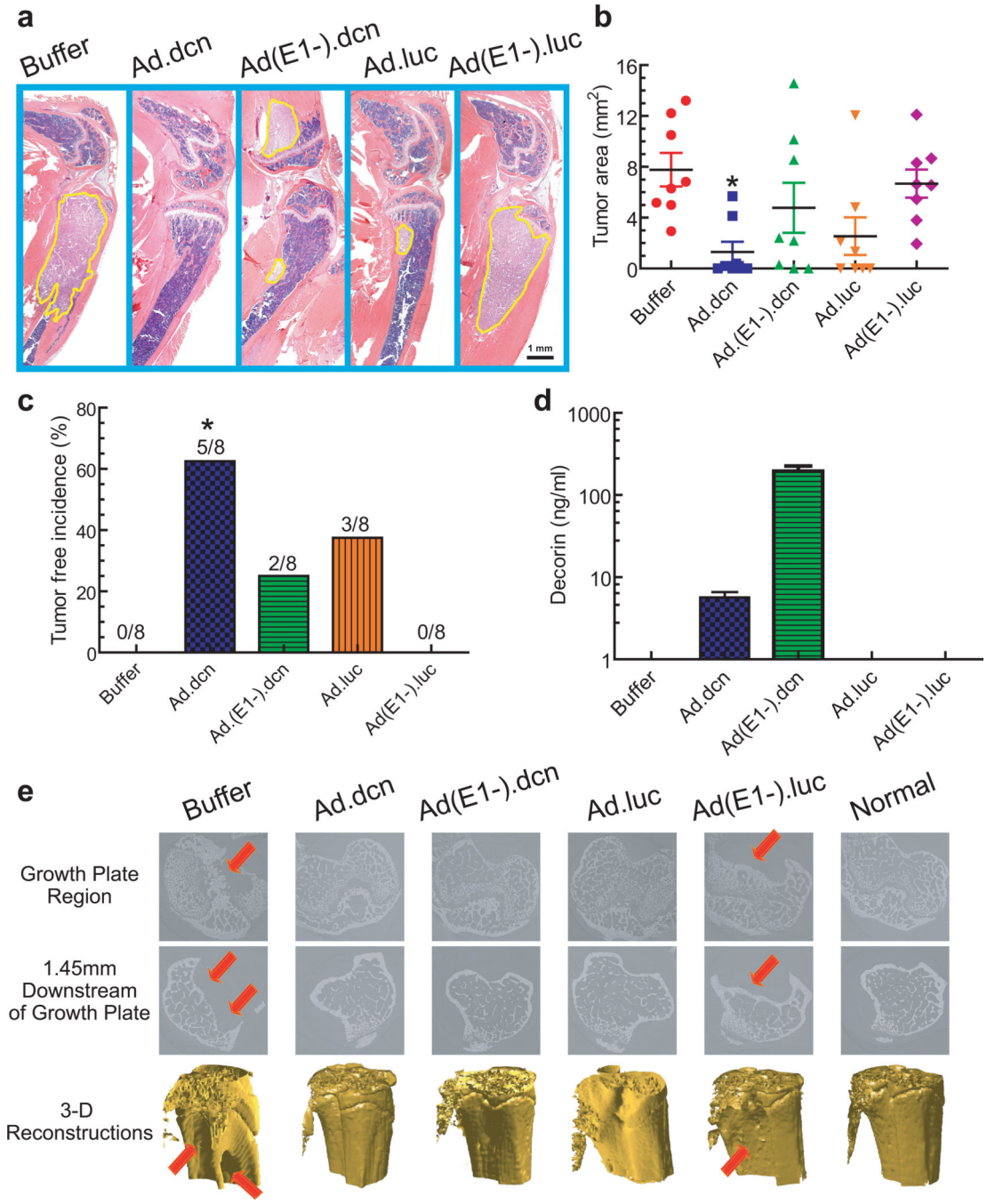

Figure 5.

Effect of adenoviral vectors on the skeletal tumor progression by histomorphometric analyses and microCT analyses. (**a**) Representative longitudinal, midsagittal H&E-stained sections of the tibia and femur (on day 62) are shown. Scale bar equals 1 mm. (**b**) Tumor areas outlined with yellow in panel (**a**) were used to measure tumor burden and are shown (n=8). (**c**) Bone metastasis free incidences (mice without histomorphometric positive lesions) on day 62 are shown (n=8). (**d**) Viral-mediated expression of decorin was measured by ELISA in mouse serum on day 62 (n=12). (**e**) Representative microCT slices near the

growth plate (top panel), 1.45 mm distal of the growth plate (middle panel), and 3-D renderings of the tibia bones form the various treatment groups (lower panel). Arrows indicate the site of bone destruction/tumor lesions. *P* value comparisons with buffer group are shown for (**b**) and (**c**) (* represents $p<0.05$).

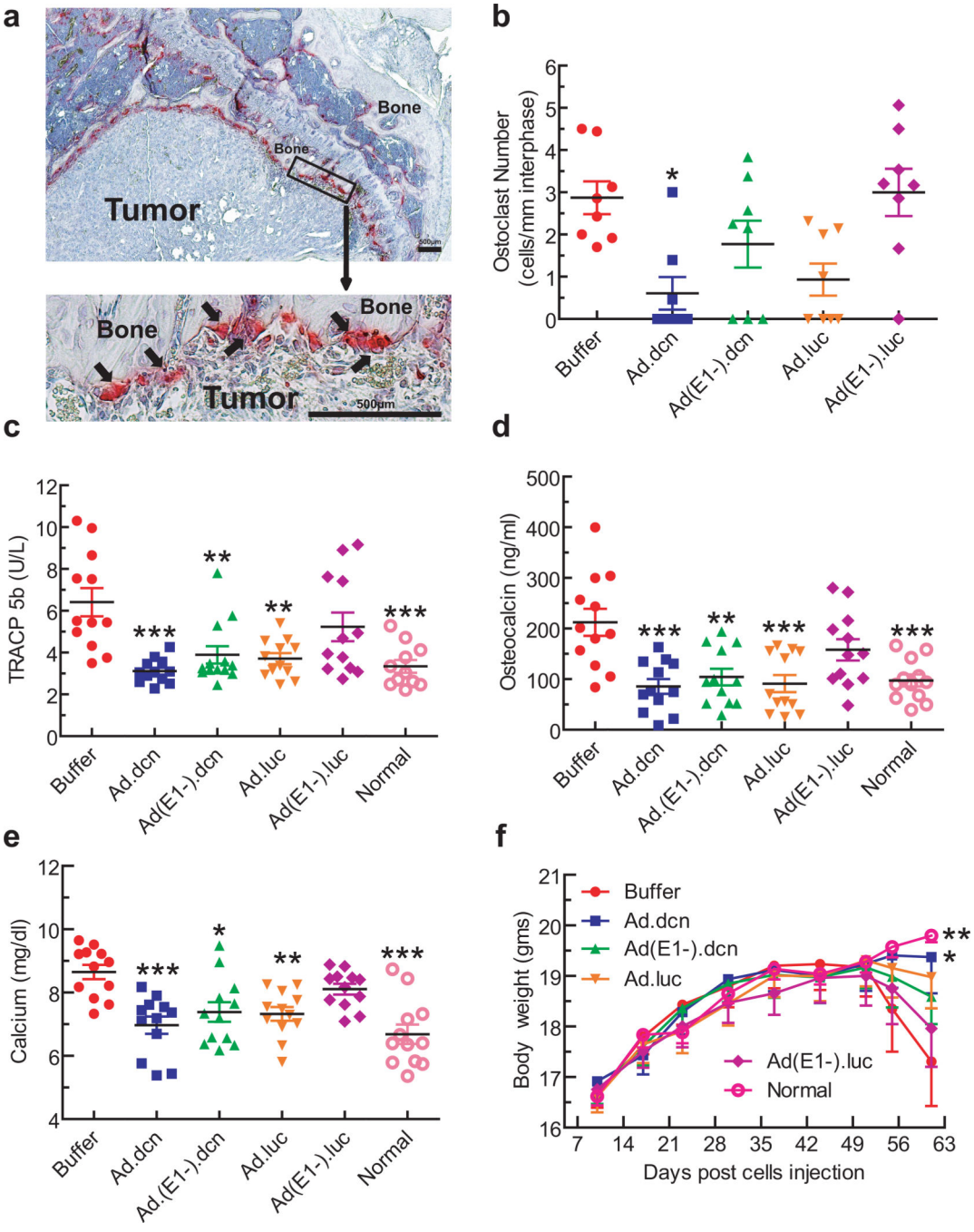

Figure 6.

Effects of adenoviral vectors on skeletal tumor progression: Osteoclast numbers, serum TRACP 5b levels, osteocalcin levels, calcium, and mice body weight analysis. (**a**) Representative TRAP staining of bone (arrows indicate multinucleated TRAP positive osteoclasts). Scale bar equals 500 μm. (**b**) Osteoclast number per mm calculated at the tumor-bone interface in each group (n=8). (**c**) Serum TRACP 5b concentration in each group (n=12) on day 62. (**d**) Serum osteocalcin concentration of all mice (n=12) on day 62. (**e**) Serum calcium concentration (n=12) on day 62. (**f**) Average body weight per group

throughout the experiment is plotted (n=12). *P* value comparisons with buffer group are shown for (**b**), (**c**), (**d**), (**e**), and (**f**) (* represents $p<0.05$, ** represents $p<0.01$, *** represents $p<0.001$).

Table 1

Summary of anti-tumor response and bone destruction assays

	BLI		X-ray			H&E		a^{+}OC	aTRACP5b	$a^{\#}$ON	aCa^{++}	bBody weight	cSurvival
	bProgression	aFold-change	bProgression	aTumor size	dTumor free	aTumor size	dTumor free						
Ad.dcn	***	**	***	*	*	*	*	*	***	***	***	*	*
Ad.(E1-)dcn	***	*	*	NS	NS	NS	NS	NS	**	**	*	NS	NS
Ad.luc	ND	*	**	NS	NS	NS	NS	NS	**	***	**	NS	NS
Ad.(E1-).luc	ND	NS	NS	NS	NS	NS	NS	NS	NS	NS	NS	NS	NS

a were analyzed by using a one-way ANOVA followed by Bonferroni post-tests.

b were analyzed statistically by using a two-way repeated-measure ANOVA followed by Bonferroni post-tests.

c were analyzed by Kaplan-Meier survival curves.

d were analyzed by Fisher exact test.

* represents $p<0.05$,

** represents $p<0.01$,

*** represents $p<0.001$;

all P values were compared with the buffer group.

$^{+}$OC is osteoclast.

$^{\#}$ON is osteocalcin.

ND represents not done.

NS represents not significant.